Materials Research. 2025; 28: e20250337
DOI: https://doi.org/10.1590/1980-5373-MR-2025-0337

Two-Step Simple Synthesis of Nanoscale Carbon Spheres via the Stöber Method Using Black Wattle Tannin as an Eco-Friendly Precursor for Supercapacitor Applications

Max Krapf Costa[a], Edna Jerusa Pacheco Sampaio[a*], Adilar Gonçalves Santos Jr[a], Andrés Cuña Suárez[b,c], Gisele Amaral-Labat[d], Célia de Fraga Malfatti[a]

[a]Universidade Federal do Rio Grande do Sul (UFRGS), Escola de Engenharia, Laboratório de Pesquisa em Corrosão (LAPEC), Porto Alegre, RS, Brasil.
[b]Universidad de la República (Udelar), Facultad de Química, Área Fisicoquímica (DETEMA), 11800, Montevideo, Uruguay.
[c]Instituto Polo Tecnológico de Pando, Facultad de Química, Universidad de la República (Udelar), Pando, Canelones, Uruguay.
[d]Instituto Nacional de Pesquisas Espaciais (INPE), 12227-010, São José dos Campos, SP, Brasil.

Received: February 25, 2025; Revised: July 15, 2025; Accepted: July 18, 2025

The growing demand for sustainable energy storage solutions has prompted the exploration of eco-friendly materials for supercapacitor applications. In this study, we present a simple two-step synthesis of nanoscale carbon spheres using a modified Stöber method, employing black wattle tannin extracted from Acacia mearnsii as a carbon precursor, in comparison with the conventional resorcinol precursor. Morphological characterization revealed that highly homogeneous nanoscale spheres were obtained. Physicochemical characterizations indicated that the tannin-derived spheres exhibited residual silica content due to incomplete template removal, which increased series resistance and limited the material's performance. Although inferior to resorcinol-derived spheres, which achieved a specific surface area of 2093 $m^2\ g^{-1}$, the tannin-derived material still exhibited a high surface area of 457 $m^2\ g^{-1}$ and a specific capacitance of 66.3 F g^{-1} in aqueous H_2SO_4 electrolyte, with well-defined morphology achieved without an activation step. By using an environmentally friendly precursor, we successfully produced a material with a homogeneous and well-defined structure, high surface area, and obtained through a simple two-step process of polymerization and carbonization without additional activation. These findings may open new directions for future research.

Keywords: *black wattle tannin, hollow carbon spheres, Stöber method, Supercapacitor electrode, green precursor, Acacia mearnsii, biomass.*

1. Introduction

Supercapacitors have been gaining prominence among energy storage devices because they can store and releasing electrical energy very quickly, which is an essential characteristic for various applications. For example, they can be used for storing renewable energy obtained from wind turbines and solar cells, as well as for electric vehicles, among other applications[1-5]. One of the essential components of supercapacitors is the electrode's active material, with carbon materials being the most studied. There are various types of carbon materials with different origins, shapes, and structures. Carbon spheres, developed in a spherical shape, can be synthesized on both nanometric and micrometric scales. These include solid spheres, spherical shells, core-shell, and yolk-shell structures[6-9]. Carbon materials in the form of hollow spheres can achieve high surface areas and exhibit high specific capacitance (95-300 $F.g^{-1}$) in aqueous electrolytes[10-14].

Carbon spheres can be developed using different techniques, such as arc discharge, laser ablation, shock compression, and chemical vapor deposition. However, these processes tend to be expensive due to the need to control parameters like pressure and temperature[6,15]. A simpler method to create carbon nanospheres is the Stöber method, which involves the hydrolysis of an alkoxide such as tetraethyl orthosilicate (TEOS)[16].

In 2011, Liu et al.[17] adapted the Stöber method by replacing the silicon precursors with a resorcinol/formaldehyde resin, resulting in mesoporous spheres with a surface area of 504 $m^2.g^{-1}$. Since then, the extended Stöber method has become widely used in the production of carbon spheres. Studies have shown that carbon spheres synthesized using a variation of the Stöber method with resorcinol as the carbon precursor exhibit a microporous structure.

In the extended Stöber method, the size, dispersion, and morphology of the spheres can be controlled by varying the concentration of the synthesis components. To produce carbon materials, incorporating resorcinol and formaldehyde is a widely used approach[17,18]. Resorcinol/formaldehyde (RF) resins are effective carbon precursors as they produce materials

*e-mail: jerusa.pacheco@ufrgs.br
Associate Editor: Jose Eiras.
Editor-in-Chief: Luiz Antonio Pessan.

with relatively high porosity and surface area, essential for use in electrochemical capacitors[19,20]. Formaldehyde acts as a crosslinking agent in the synthesis of carbon nanospheres, facilitating the polymerization reaction and forming a three-dimensional structure.

In designing hollow carbon spheres for core-shell structures, resorcinol-formaldehyde (RF) resin is commonly used as a carbon source due to its affordable cost, simple polymerization process, and high residual carbon content[21]. Antonio B. Fuertes et al.[22] were the first to produce core-shell spheres composed of a thin layer of RF resin surrounding a silica core using a one-step method under Stöber conditions. This process resulted in spheres with a surface area of 720 $m^2.g^{-1}$. Such structures create opportunities for developing new designs of carbon spheres for various applications, particularly in electrochemical energy storage.

Resorcinol is an organic chemical compound highly soluble in water. It is widely used in various industries, including in the manufacture of polymers, rubbers, dyes, coatings, and dermatological products. Despite its widespread use, high concentrations or excessive use of resorcinol can be harmful to health, causing skin lesions and impairing the respiratory system[23,24]. Reducing the cost of materials and processes, as well as finding materials that do not harm the environment and human health, is of fundamental importance.

Tannin has emerged as a promising alternative for synthesizing carbon materials with high porosity. Tannin is a natural and inexpensive product found in various plants, including leaves, tree bark, roots, and fruits[25]. These polyphenolic biomolecules have a high carbon content, which varies depending on their plant source[26].

Studies showed that the raw material for tannin significantly influenced the obtained structures. Beda et al.[27] proposed an optimization study of hard carbon spheres derived from tannin for sodium-ion battery applications. They demonstrated that the particle size could be adjusted from 4.1 μm to ~0.4 μm by changing the polyphenol source from Catechu to Mimosa, while the morphology changed from interconnected particles to individual particles. Another alternative tannin eco-friendly carbon precursor is black wattle (Acacia mearnsii), particularly interesting due to its high tannin content and well-established industrial extraction method. Black wattle was used as a tannin precursor for anti-fouling pigment, corrosion inhibitor, carbon xerogel as a co-catalyst in solar light-based photocatalytic processes, adsorbent for removing pharmaceuticals from aqueous environments, among other applications[28-31]. Braghiroli et al.[32] produced nitrogen-doped carbon microspheres from black wattle tannin precursor via hydrothermal route, which were then carbonized at 900 °C, resulting in an essentially microporous material with a surface area of 640 m^2 g^{-1} without additional activation, revealing a new and promising raw material for preparing new carbon materials.

Studies using tannin as a carbon precursor have shown promising results, with surface areas between 510 and 1810 $m^2.g^{-1}$ [25,33]. In another study, polystyrene spheres were synthesized as templates through emulsion polymerization using potassium persulfate as the initiator. Tannin was then added in a sol-gel process to develop hollow carbon spheres, achieving a surface area of up to 1971 $m^2.g^{-1}$ and a capacitance of 265 $F.g^{-1}$ [34]. Despite these significant surface area and electrochemical performance values, the synthesis process is lengthy, requiring approximately eight days of processing.

The extended Stöber method has also shown promise in producing carbon spheres from tannin-based precursors. Liu et al.[35] developed solid spheres using the Stöber method with tannic acid as the carbon precursor. In this study, a surface area of 327 $m^2.g^{-1}$ was achieved.

Regarding the desirable characteristics for materials applied to supercapacitors, surface area is mandatory. The literature indicates that activation processes can considerably maximize the surface area of spheres produced by the Stöber method. However, while it is possible to maximize the surface area to values exceeding 2000 $m^2.g^{-1}$ after physical or chemical activation, these processes require treatment at high temperatures, ranging from 600 °C to 1000 °C. Yang et al. reported the synthesis of carbon spherical particles (SCs) using the Stöber method. A surface area of 503.2 $m^2.g^{-1}$ was obtained, which increased to 712 $m^2.g^{-1}$ after thermal treatment. Subsequently, surface areas of 2050.6 $m^2.g^{-1}$ and 2152.9 $m^2.g^{-1}$ were achieved after high-temperature activation with KOH and CO_2, respectively[36]. On the other hand, Liu et al.[37] demonstrated a facile and controllable synthesis of N-doped carbon spheres by an amine-induced Stöber-silica/carbon method using resorcinol as a precursor, achieving a surface area of up to 2001 m^2 g^{-1} without an activation step, indicating the great potential of this method to produce carbon nanospheres.

In this study, nanoscale carbon spheres with high surface area were produced using a simple two-step route based on the extended Stöber method, without further activation. Two carbon precursors were investigated: resorcinol, traditionally employed in the literature for this method, and black wattle tannin (extracted from Acacia mearnsii) as an alternative eco-friendly precursor.

2. Material and Methods

2.1. Synthesis of the carbon spheres

Carbon spheres were prepared using the Stöber method with a silica precursor as a template to achieve structures[38,39]. The synthesis began by adding 9.0 mL of NH_4OH to a solution containing 30 mL of deionized water and 210 mL of ethanol. The solution was mixed using a magnetic stirrer for 10 minutes at room temperature (23 °C). After this initial step, 6 mL of TEOS was added, and the mixture was stirred for 40 minutes at 40 °C. Following this 40-minute period, in the resorcinol version, 1.5 g of resorcinol and 3 g of formaldehyde were added. In the alternative method, black wattle tannin precursor was used, which was provided by TANAC, a Brazilian manufacturer of sustainable bio-products derived from renewable forest resources. In this version, 1.5 g of black wattle tannin and 3 g of formaldehyde were added to the initial TEOS mixture, the solutions underwent magnetic stirring for an additional 24 hours at 40 °C.

Subsequently, the material was washed and separated using a centrifuge, followed by drying in an oven at 80 °C for 24 hours. The dried material underwent thermal treatment in a tubular furnace for 3 hours under N_2 flow at 700 °C. Subsequently, the silica templates were removed by an

alkaline etching treatment, a 4 M NaOH solution was used, and the material was stirred at 23 °C for 24 hours. After the template removal, the material was washed with deionized water and separated using a centrifuge. The material was then dried in an oven at 80 °C for 24 hours and considered ready for physicochemical characterization and electrode preparation.

The sample produced using tannin was named TAN, and the sample with resorcinol was named RES. For comparison, commercial activated carbon NORIT® was also characterized with samples named CA.

2.2. Physicochemical characterization

In this study, Raman spectra were collected using a Horiba Scientific LabRAM HR Evolution spectrometer. The measurements were carried out with an Ar+ laser operating at a wavelength of 514.6 nm and a power of 10 mW. The laser was focused onto the sample through an optical microscope, and extended spectral scans were performed over the range of 800 to 2200 cm^{-1}, with an exposure time of 30 seconds for each measurement.

Nitrogen adsorption-desorption measurements were conducted using an ASAP 2020 PLUS system (Micromeritics®) over a relative pressure range (P/P_0) from 10^{-6} to 0.99. Before analysis, the samples were degassed at 200 °C for 24 hours under vacuum to remove any residual moisture or adsorbed gases. The specific surface area was determined using the Brunauer-Emmett-Teller (BET) method[40], while the pore size distribution was calculated using the density functional theory (DFT) model. The total pore volume ($V_{0.97}$) was estimated based on the volume of liquid nitrogen adsorbed at a relative pressure of $P/P_0 = 0.97$ ($cm^3\ g^{-1}$)[41]. The micropore volume (V_{DR}) was calculated using the Dubinin-Radushkevich (DR) method[42], and the mesopore volume (Vmeso) was obtained by subtracting V_{DR} from the total volume at $P/P_0 = 0.97$.

The morphological and elemental characterization of the samples was performed using a TESCAN MIRA3 tungsten filament scanning electron microscope (SEM) equipped with an energy-dispersive X-ray spectroscopy (EDS) system. All samples were analyzed without any additional surface treatment or coating. The SEM was operated at an accelerating voltage of 5.0 kV, with a working distance of approximately 5 mm. During imaging, secondary electrons (SE) and backscattered electrons (BSE) were collected to generate high-resolution micrographs. Elemental analysis was conducted using an EDX detector integrated with the SEM and the resulting spectra were processed using the Oxford Aztec 3.0 software.

2.3. Electrochemical characterization

The performance of the materials as supercapacitor electrodes was evaluated through electrochemical characterization in a two-electrode symmetrical cell using a 1 M aqueous solution of sulfuric acid as the electrolyte. The electrode material was prepared as follows: the powdered material under analysis (80%) was mixed with Vulcan carbon (10%) and PTFE binder (10%). The materials were mixed using a magnetic stirrer for 3 hours in a beaker containing ethanol at 40 °C.

After mixing, the suspension was pipetted onto graphite rods (current collectors) with a diameter of 6 mm and placed in an oven where they remained for 24 hours, resulting in 1.5 mg of material deposited on the surface of each electrode.

Cyclic voltammetry (CV) and galvanostatic charge-discharge (GCD) experiments were conducted in the potential range of 0 to 1 V, at different scan rates (10, 20, and 50 $mV.s^{-1}$) and current densities, respectively. All experiments were performed at room temperature (23°C) using an AUTOLAB PGSTAT302 N potentiostat/galvanostat. The capacitance was determined from the charge-discharge curves using Equation 1:

$$Cs = \left(4*i*\Delta t\right) / \left(\Delta V*m\right) \quad (1)$$

where C ($F\ g^{-1}$) is the capacitance, I (A) is the discharge current, Δt (s) is the discharge time, ΔV (V) is the discharge potential, and m (g) is the mass of the electrodes[43]. The energy density and specific power of the device were calculated using Equations 2 and 3, where C is the capacitance, V is the operating voltage, E represents the energy of the device, and t is the discharge time[44].

$$E = \left(C*V2\right) / 2 \quad (2)$$

$$P = E / t \quad (3)$$

3. Results

3.1. Physicochemical characterizations

The morphology of the synthesized nanospheres was investigated using SEM. Figure 1 depicts micrographs of the RES sample at two magnifications, revealing homogeneous carbon spheres successfully obtained. The spheres were clustered together with uniform sizes of approximately 440 nm in diameter. Similarly, Figure 2 shows SEM images of the TAN version samples, developed using tannin as the carbon precursor. The micrographs reveal well-defined spheres on the nanoscale with a homogeneous and spherical shape. The TAN spheres exhibit a smaller diameter of approximately 346 nm compared to the RES samples and contain residual material inside the spheres. Figure 3 presents SEM images of the sample with commercial activated carbon, used as a benchmark in the electrochemical measurements.

Raman spectroscopy analysis was conducted in the range of 750 cm^{-1} to 2250 cm^{-1}, as shown in Figure 4, to study the vibrational behavior of the carbon materials. The presence of peaks corresponding to the D and G bands at approximately 1350 cm^{-1} and 1510 cm^{-1}, respectively, confirms the presence of amorphous carbon. The ID/IG ratio for all samples, presented in Table 1, indicates characteristics of amorphous material.

Energy Dispersive X-ray Spectroscopy (EDS) analysis reveals the chemical composition of the samples, as shown in Figures 5a-c. The RES samples exhibit very low silica content, aligning with the SEM analysis, which indicates no encapsulated silica-related material inside the carbon spheres. In contrast, TAN samples show high silica content, likely residual material due to incomplete removal during the etching step. Based on SEM and EDS analyses, the

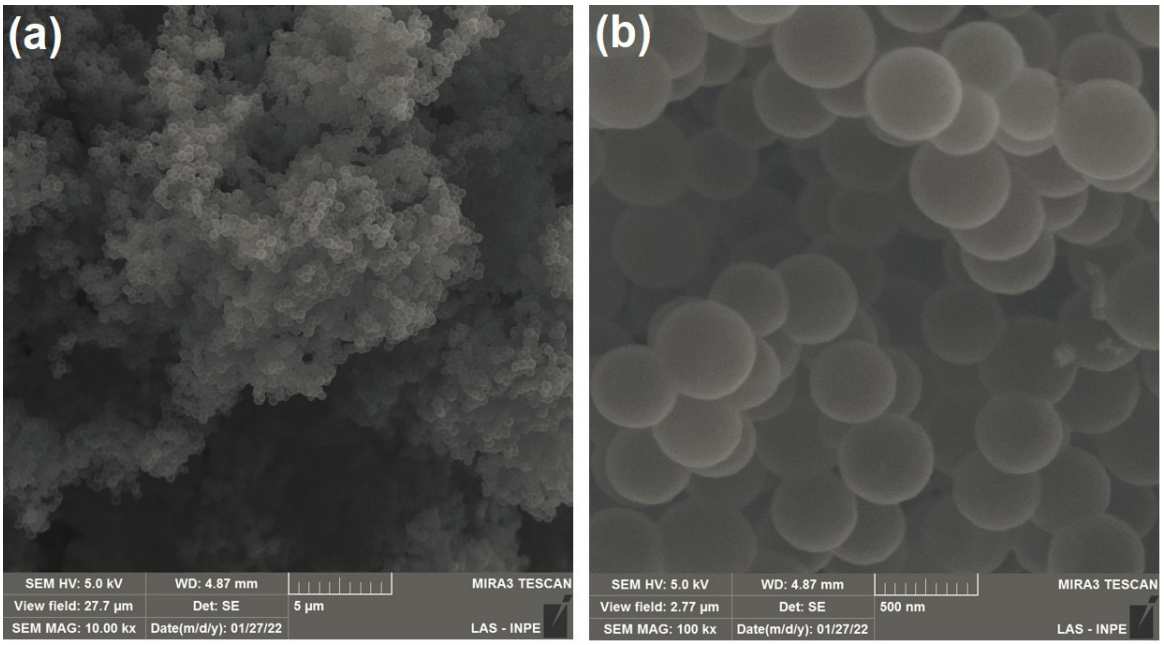

Figure 1. SEM images of the RES sample with magnification of (a) 10kx and (b) 100kx.

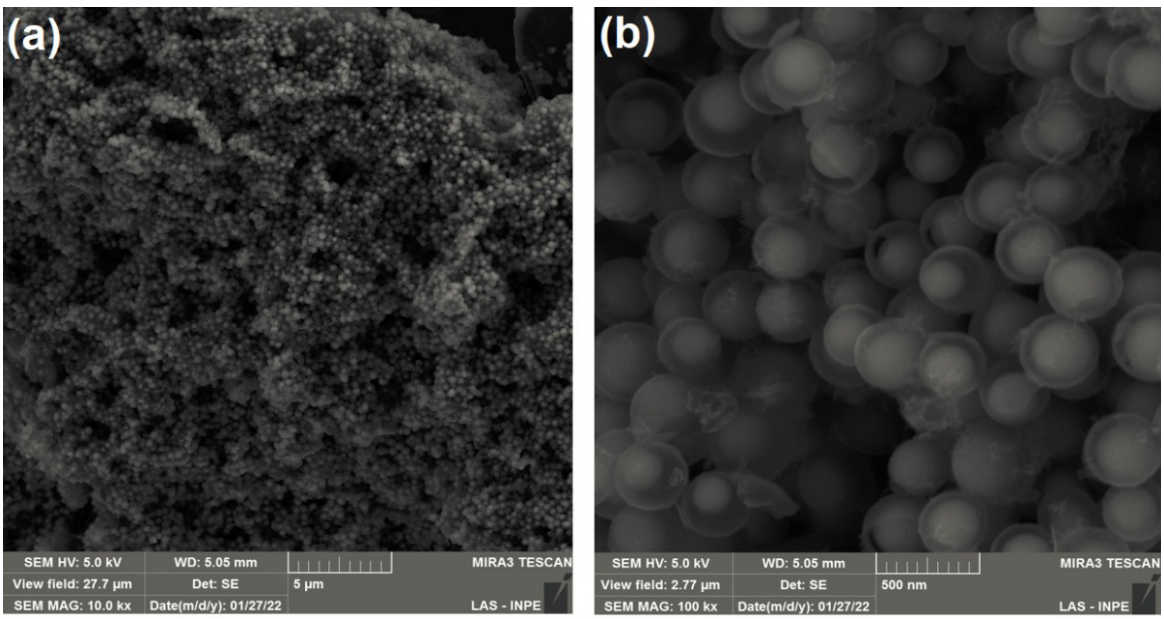

Figure 2. SEM images of the TAN sample with magnification of (a) 10kx and (b) 100kx.

material observed inside the TAN spheres is inferred to be residual silica. The complete composition of each version is detailed in Table 2.

The specific surface area (S_{BET}) of the spheres was investigated using the BET method with nitrogen adsorption-desorption isotherms at 77 K, and the results are summarized in Table 3. The RES version exhibited an ultra-high surface area of 2093 $m^2 g^{-1}$, with a total pore volume of 2.10 $cm^3 g^{-1}$. The micropores contributed 49% and mesopores 51%. In contrast, the TAN version exhibited a surface area of 457 $m^2 g^{-1}$, significantly lower than the RES version, and a total pore volume of 0.26 $cm^3 g^{-1}$, with 70% micropores and 30% mesopores.

3.2. Electrochemical measurements

Figures 6(a) and 6(b) display comparative cyclic voltammetry (CV) curves obtained in a 1 M aqueous H_2SO_4 electrolyte with scan rates of 10, 20, and 50 mV s^{-1} within a potential window of 0 to 1 V. Figure 6(a) illustrates the CV curves of the RES and TAN samples at different scan rates,

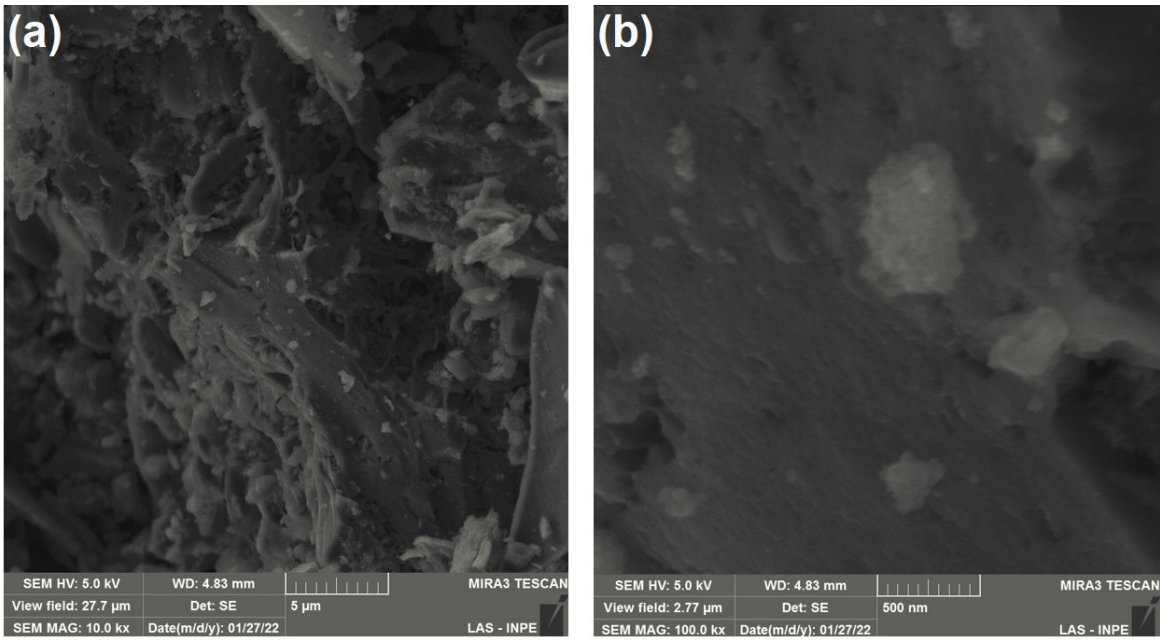

Figure 3. SEM images of the CA sample with magnification of (a) 10kx and (b) 100kx.

while Figure 6(b) compares CV curves at 50 mV s^{-1} of these samples with commercially used activated carbon (CA). All measurements were conducted on materials without prior electrochemical testing, and all tested samples exhibited capacitive behavior. The CV curves of the RES and TAN versions demonstrated a nearly rectangular shape.

Figure 7 shows the GCD curves of the RES, TAN, and CA samples at current densities of 1 A g^{-1} and 2 A g^{-1}. These curves exhibited triangular shapes. A noticeable slope during the charging stage was observed in the RES and TAN samples, contrasting with the CA version.

The Equivalent Series Resistance (ESR) values were calculated from the initial potential drop during discharge and are shown in Table 4, at current densities ranging from 1 to 4 A g^{-1}. Table 4 also presents the capacitance values of the samples, calculated based on the discharge time using Equation 1. Figure 8 depicts the relationship between capacitance and current density, highlighting variations in capacitance retention among the tested materials.

Energy density (Wh kg^{-1}) and power density (W kg^{-1}) were determined for the RES, TAN, and CA samples and are shown in Figure 9. Calculations were based on Equations 2 and 3, with adjustments made to account for the symmetric supercapacitor configuration. The RES sample exhibited the highest performance, with an energy density of 7.2 Wh kg^{-1} at a power density of 0.62 kW kg^{-1} and a maximum power density of 2.5 kW kg^{-1} at 4 A g^{-1}. The TAN sample demonstrated an energy density of 2.3 Wh kg^{-1} under the same power density and a maximum power density of 2.5 kW kg^{-1} at 4 A g^{-1}.

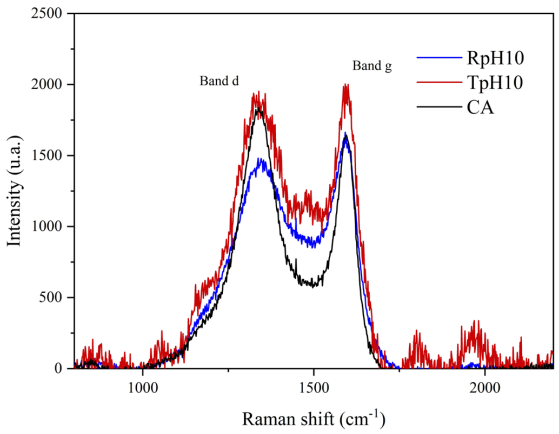

Figure 4. Raman Spectra of the RES, TAN, and CA samples.

4. Discussion

4.1. Physicochemical characterizations

The homogeneous and spherical morphology observed in both the RES and TAN samples confirms the successful synthesis of carbon spheres. Many templating methods used for the synthesis of porous carbons often result in a significant length-scale gap between meso- and macropores, typically ranging from 10 to 1000 nm[47]. The Stöber method is widely recognized for providing control and uniformity in structure size, was adapted in this study to incorporate a green precursor as an alternative to the conventional and hazardous resorcinol. The toxicity of chemical compounds is commonly evaluated by determining the oral LD_{50} value in a suitable experimental animal model. This value indicates the estimated dose expected to cause mortality in 50% of the exposed subjects. Resorcinol has been reported to have an oral LD_{50} in rats of 301 mg/kg, suggesting a moderate level of toxicity[48]. Compared to the toxicity and handling risks of resorcinol, tannins represent a safer, low-cost, and eco-friendly precursor, rich in polyflavonoids (up to 80%), and have shown excellent potential to produce porous carbon[49].

Table 1. Raman Shift Data for RES, TAN, and CA Samples.

Sample	D-Band	G-Band	I_D/I_G
	I_D (u.a)	I_G (u.a)	
RES	1468	1615	0.90
TAN	1915	1966	0.97
CA	1821	1631	1.11

Table 2. Elemental Composition from EDS Analysis.

Sample	Carbon wt%	Oxygen wt%	Sodium wt%	Silicon wt%	Chlorine wt%	Sulfur wt%
RES	89.2	9.7	0.8	0.2	0.2	-
TAN	42.1	39.1	0.6	18.1	-	-
CA	92.2	7.6	-	0.1	-	0.1

Table 3. Dimensional characteristics, pore structures, and specific surface areas.

Sample	S_{BET}, $m^2 g^{-1}$	Ø Sphere Nm	Ø pore Nm	$V_{0.97}$ $cm^3 g^{-1}$	V_{DR} $cm^3 g^{-1}$	V_{meso} $cm^3 g^{-1}$	V_{DR} / $V_{total\ 0.97}$	V_{meso} / $V_{total\ 0.97}$	Ref.
RES	2093	440	4.0	2.10	1.02	1.08	0.49	0.51	This work
TAN	457	356	2.3	0.26	0.18	0.08	0.70	0.30	
CA	1234	-	2.5	0.76	0.49	0.27	0.65	0.35	
Larch Bark Tannins	236	-	-	0.1	0.088	0.012	0.88	0.12	[33]
Tannic acid–formaldehyde	327	470	-	-	-	-	-	-	[35]
Tannin-derived hard carbon spheres	11.2 6	450 3200	-	-	-	-	-	-	[45]
Resorcinol Carbon Spheres	416	500	2.1	-	-	-	-	-	[46]

V_{DR} = micropore volume; V_{meso} = mesopore volume

Table 4. Results of capacitance and resistance of the samples versions RES, TAN and CA at different current densities.

Sample	1 $A.g^{-1}$		2 $A.g^{-1}$		3 $A.g^{-1}$		4 $A.g^{-1}$	
	Capacitance (F)	**ESR** (Ω)	**Capacitance** (F)	**ESR** (Ω)	**Capacitance** (F)	**ESR** (Ω)	**Capacitance** (F)	**ESR** (Ω)
RES	208.8	7.9	150.5	10.0	120.8	9.2	99.0	8.8
TAN	66.3	22.7	38.5	25.4	21.8	24.5	10.0	23.7
CA	130.8	4.3	117.5	4.2	108.0	3.8	101.2	4.0

The smaller diameter of the TAN spheres compared to the RES spheres could be attributed to differences in the carbon precursor used. The presence of material inside the TAN spheres, identified as residual silica, aligns with the incomplete etching process during synthesis. These findings are consistent with previous reports on carbon sphere synthesis[50].

The D and G bands observed in the Raman spectra confirm the amorphous nature of the synthesized carbon materials. The I_D/I_G ratio supports this finding, as amorphous carbon typically exhibits higher values than crystalline graphite. The vibrational behavior of the developed materials aligns with established characteristics of carbon nanospheres[51]. Amorphous carbons exhibit advantageous properties such as intrinsic isotropy, abundant active sites, structural flexibility, and rapid ion diffusion, making them highly promising for electrochemical energy storage and conversion. Compared to their crystalline counterparts, amorphous materials experience less significant volume variation due to a higher number of intercalation sites resulting from their internal defects and disorder. As a result, these materials enable rapid ion transport and ensure greater structural stability due to their extensive network of ion transport pathways and flexible packing[52].

The high silica content observed in TAN samples through EDS analysis suggests residual material from the silica template used during synthesis. The absence of significant silica content in RES samples correlates with their higher surface area and pore volume, as the removal of silica templates appears more effective in these samples. These results underscore the importance of optimizing the etching process to enhance the purity and performance of carbon spheres.

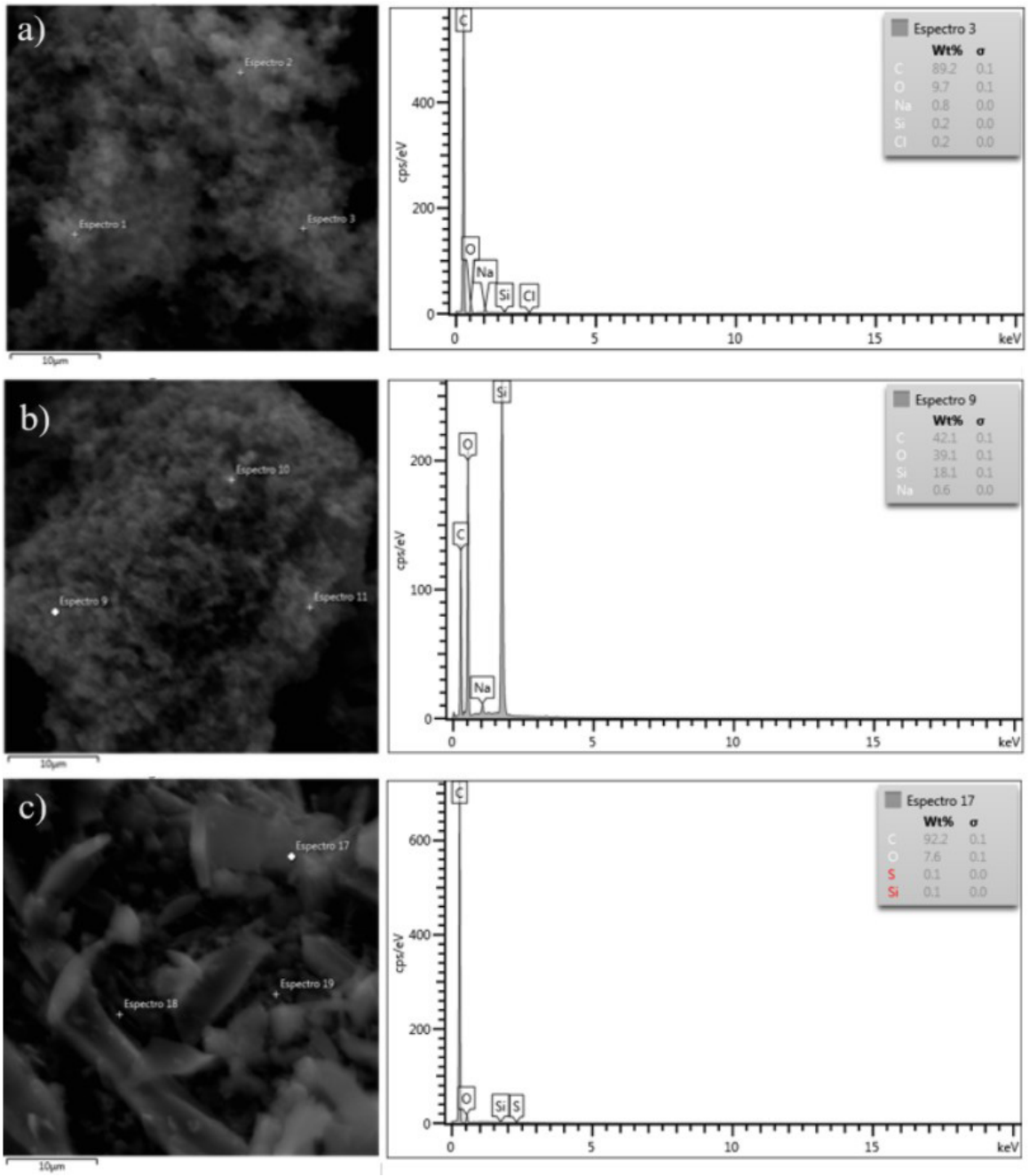

Figure 5. Energy-Dispersive X-ray Spectroscopy of: a) RES, b) TAN, and c) CA.

The significantly higher surface area and pore volume of the RES version compared to the TAN version can be attributed to the lower silica content in the RES samples. Residual silica in TAN samples likely obstructs the pores, reducing their surface area and total pore volume. Despite this limitation, the TAN version achieves a surface area higher than those reported in studies using alternative methods for tannin-based sphere synthesis[50,53]. The comparison to resorcinol-based carbon spheres prepared with different catalytic sources further highlights the promising characteristics of the TAN version[45,46].

BET results demonstrated that tannin is a promising precursor for synthesizing carbon nanospheres via the modified Stöber method. Notably, a relatively high surface area was achieved despite the presence of residual silica in the tannin-derived samples. In contrast, other methods such as tannin hydrothermal carbonization (HTC) without additional pyrolysis typically yield carbon microspheres with a pearl-necklace morphology and low surface areas around 60 $m^2 g^{-1}$. While additional pyrolysis steps are often needed to enhance porosity, even more sophisticated routes—like the preparation of tannin-formaldehyde (TF) cryogels through freeze-drying and pyrolysis—only result

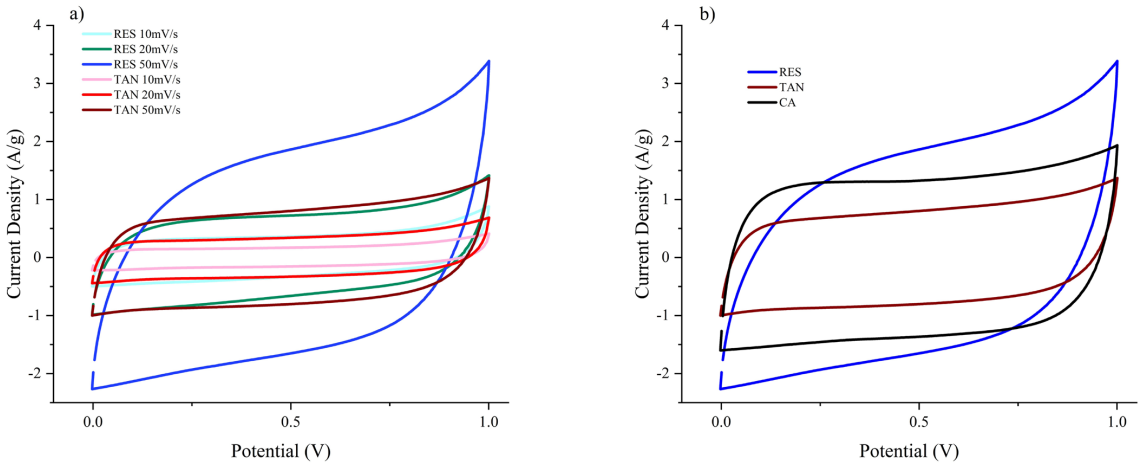

Figure 6. Cyclic Voltammogram curves a) TAN and RES at various scan rates. b) TAN, RES, and commercial activated carbon at a scan rate of 50 mV s^{-1}.

in high surface areas when synthesized at pH above 6 and still lack significant mesoporosity. Recent advances using mechanosynthesis approaches have produced tannin-derived carbons with surface areas around 500 m^2 g^{-1} [54], although larger areas generally require an additional activation step with CO_2 [55]. Other studies using tannin-derived precursors have reported specific surface areas of 237 m^2 g^{-1} for sol-gel synthesized tannin-based spheres[33], and 327 m^2 g^{-1} for spheres prepared from tannic acid and formaldehyde using the Stöber method[35].

The specific surface area of 457 m^2 g^{-1} for the biobased carbon spheres through a straightforward carbonization process under an inert atmosphere, without requiring subsequent activation, emphasizes the intrinsic porosity and favorable structural features, achieved by the modified Stöber synthesis. This approach demonstrates an efficient and facile route for synthesizing moderate surface-area carbon nanomaterials from renewable precursors.

4.2. Electrochemical measurements

The electrochemical performance of the RES and TAN samples confirms their double-layer capacitance behavior, as evidenced by the nearly rectangular CV curves and triangular GCD profiles. The absence of current peaks in the voltammetry curves indicates that no significant redox reactions occurred. This suggests that charge storage is dominated by double-layer capacitance rather than pseudocapacitance, as pseudocapacitive materials typically exhibit clear redox peaks[55,56].

The RES and TAN samples exhibit a steeper slope during the charging stage compared to the CA version, likely due to the inherent resistance in these versions, causing them to take more time to reach the 1 V voltage. In GCD curves the potential experiences a drop at the beginning of the discharge process, followed by stabilization. This drop is due to the resistance of ions moving toward or away from the electrodes, as well as the processes at the electrode-electrolyte interface. This phenomenon is linked to the internal resistance of the components, which is influenced by factors such as electrode structure, electrolyte type, and the quality of electrical contacts[57,58].

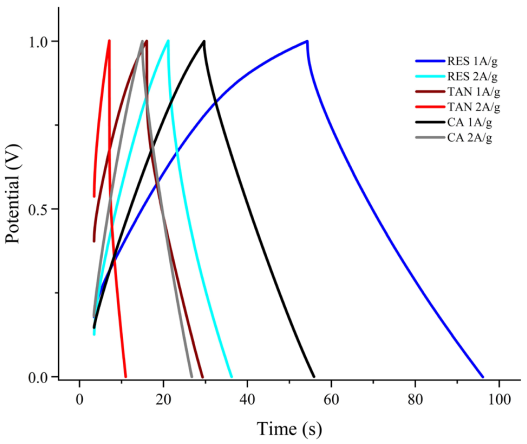

Figure 7. Galvanostatic Charge and Discharge curves of the RES, TAN and CA samples at 1 A g^{-1} and 2 A g^{-1}.

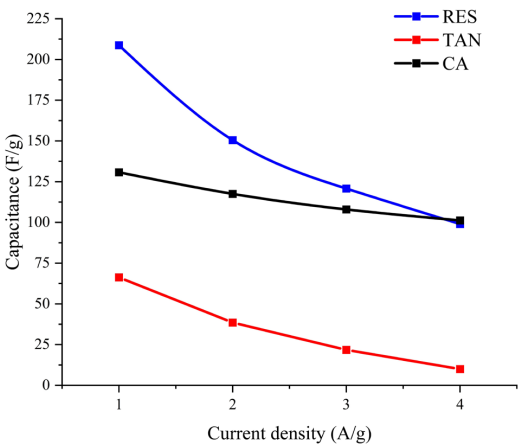

Figure 8. Capacitance retention curves as a function of current density.

The ESR values for the RES range from 7.9 Ω to 8.8 Ω, suggesting moderate resistance attributed to the material's structure compared to the CA benchmark sample. The TAN exhibits the highest ESR values, ranging from 22.7 Ω to 23.7 Ω, which can be attributed to the presence of residual silica impairing the material conductivity. These characteristics contribute to the limitations observed in its electrochemical performance.

In terms of energy density *vs* power density, RES version demonstrated the highest performance among the tested samples, with an energy density of 7.2 Wh kg^{-1} at a power density of 0.62 kW kg^{-1}, measured at a current density of 1 A g^{-1}. Furthermore, it reached a maximum power density of 2.5 kW kg^{-1} at 4 A g^{-1}. These results highlight the superior charge storage capacity of the RES version, likely due to its higher surface area and optimized pore distribution, as previously discussed. In contrast, the TAN version exhibited a maximum energy density of 2.3 Wh kg^{-1} at the same power density of 0.62 kW kg^{-1}, measured under identical conditions. Its maximum power density of 2.5 kW kg^{-1} at 4 A g^{-1} matches that of the RES version, indicating comparable high-rate performance even when compared to commercial activated carbon as can be seen in Figure 9. However, the lower energy density of the TAN sample can be attributed to residual silica blocking the pores, as observed in the SEM and EDS analyses. This limitation reduces the effective surface area available for charge storage, impairing its energy density despite the material's inherent capacitive behavior. These results suggest that the electrochemical performance can be further improved by optimizing the etching process to ensure complete silica removal. Additionally, strategies such as heteroatom doping of tannin-derived carbon spheres show great promise, as they can facilitate fast Faradaic reactions and enhance pseudocapacitance. Recent studies also highlight that chemical activation of tannin-based carbons using K_2CO_3 significantly increases their specific surface area and capacitive behavior[59,60,61].

Furthermore, the approach presented in this study is consistent with the United Nations Sustainable Development Goals (SDGs), notably SDG 7 (Affordable and Clean Energy), by facilitating the advancement of environmentally sustainable energy technologies. Using renewable biomass and decreasing dependence on synthetic chemicals, such as resorcinol, directly contributes to SDG 12 (Responsible Consumption and Production), promoting more sustainable and eco-friendly industrial processes. Additionally, valorizing natural resources and developing innovative energy storage materials support SDG 9 (Industry, Innovation, and Infrastructure), advancing technological innovation with clear environmental and societal impacts[62]. Therefore, this study not only contributes to the field of materials science but also highlights a dedication to sustainable development aligned with the global objectives established by the United Nations.

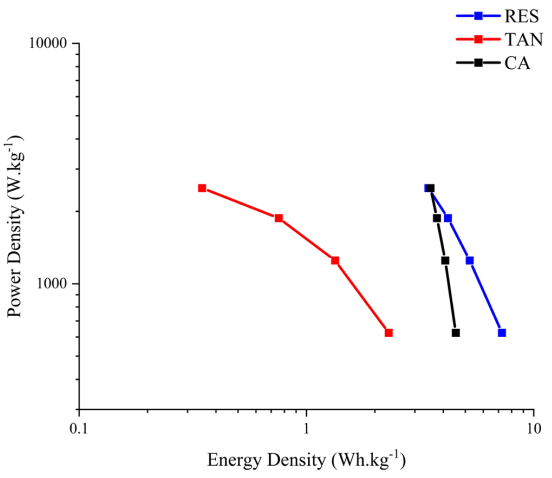

Figure 9. Ragone plot showing energy and power density curves of the RES, TAN and CA.

5. Conclusion

In this study, porous carbon spheres were successfully synthesized using black wattle tannin as a natural alternative to resorcinol in the Stöber method, aiming energy storage applications. SEM analysis confirmed the formation of spherical morphologies for both precursors. However, tannin-derived spheres showed residual core material and lower uniformity compared to resorcinol-derived ones. EDS analysis also revealed high silicon content in the tannin-based sample, suggesting incomplete silica removal.

Despite these limitations, nitrogen adsorption–desorption analysis showed that both materials exhibited high surface areas, with 2093 $m^2 \cdot g^{-1}$ for the resorcinol-based carbon and 457 $m^2 \cdot g^{-1}$ for the tannin-based carbon. These results are noteworthy considering that such values were obtained without any additional chemical or thermal activation steps. The two-step synthesis method, consisting of polymerization followed by carbonization, proved to be a simple and effective approach for producing porous carbon spheres with high surface area, even when using a plant-based precursor.

Electrochemical tests revealed superior capacitive behavior for the resorcinol-derived sample. In contrast, the tannin-based material exhibited lower current responses, likely due to residual silica that may have partially obstructed the pore network. Nevertheless, the study demonstrates that tannin can serve as a viable carbon precursor for producing high surface area porous structures and highlights the influence of precursor type and synthesis parameters on the resulting material properties.

The results of this study indicate that tannin can be used as a carbon precursor for porous carbon spheres the synthesis, although its performance in energy-related applications remains limited compared to resorcinol-derived materials. Nonetheless, homogeneous nanoscale carbon spheres were successfully synthesized from this natural precursor using a modified Stöber method. The approach contributes to the development of more sustainable synthesis routes by employing renewable biomass and reducing reliance on synthetic precursors such as resorcinol.

This strategy is aligned with efforts to promote environmentally responsible practices and the valorization of natural resources in the development of carbon-based functional materials

6. Acknowledgments

The authors are grateful for the financial support of CAPES Brazilian Government entities focused on human resources formation (PROEX 88881.844968/2023-01) and CNPq—National Council for Scientific and Technological

Development (TO 405948/2022-0). C. F. Malfatti thanks CNPq (Grant. 313493/2023-5), Adilar Gonçalves dos Santos Jr thanks CNPq (Grant. 351108/2023-8), Gisele Amaral-Labat thanks CNPq (Grant. 301364/2024-9) and Edna Jerusa Pacheco Sampaio thanks CNPq (Grant 350271/2024-0).

7. References

1. Şahin ME, Blaabjerg F, Sangwongwanich A. A comprehensive review on supercapacitor applications and developments. Energies. 2022;15(3):674. http://doi.org/10.3390/en15030674.
2. Subasinghage K, Gunawardane K, Padmawansa N, Kularatna N, Moradian M. Modern Supercapacitors technologies and their applicability in mature electrical engineering applications. Energies. 2022;15(20):7752. http://doi.org/10.3390/en15207752.
3. Prasad GG, Shetty N, Thakur S, Rakshitha, Bommegowda KB. Supercapacitor technology and its applications: a review. IOP Conf Ser: Mater Sci Eng. 2019;561(1):012105. http://doi.org/10.1088/1757-899X/561/1/012105.
4. Kealy T. The need for energy storage on renewable energy generator outputs to lessen the Geeth effect, i.e. short-term variations mainly associated with wind turbine active power output. Energy Rep. 2023;9:1018-28. http://doi.org/10.1016/j.egyr.2022.12.040.
5. Dissanayake K, Kularatna-Abeywardana D. A review of supercapacitors: materials, technology, challenges, and renewable energy applications. J Energy Storage. 2024;96:112563. http://doi.org/10.1016/j.est.2024.112563.
6. Deshmukh AA, Mhlanga SD, Coville NJ. Carbon spheres. Mater Sci Eng Rep. 2010;70(1):1-28. http://doi.org/10.1016/j.mser.2010.06.017.
7. Cao KLA, Iskandar F, Tanabe E, Ogi T. Recent advances in the fabrication and functionalization of nanostructured carbon spheres for energy storage applications. Kona. 2023;40(0):197-218. http://doi.org/10.14356/kona.2023016.
8. Hussain I, Sahoo S, Sayed MS, Ahmad M, Sufyan Javed M, Lamiel C, et al. Hollow nano- and microstructures: mechanism, composition, applications, and factors affecting morphology and performance. Coord Chem Rev. 2022;458:214429. http://doi.org/10.1016/j.ccr.2022.214429.
9. Li L, Wang C, Zhang C, Cao X, Bai J, Li R. Yolk-shell V2O3/nitrogen-doped carbon spheres as an ultra-long life anode for half/full sodium-ion batteries. J Energy Storage. 2023;66:107504. http://doi.org/10.1016/j.est.2023.107504.
10. Fang X, Zang J, Wang X, Zheng MS, Zheng N. A multiple coating route to hollow carbon spheres with foam-like shells and their applications in supercapacitor and confined catalysis. J Mater Chem A Mater Energy Sustain. 2014;2(17):6191-7. http://doi.org/10.1039/c3ta14881e.
11. Dai Y, Jiang H, Hu Y, Fu Y, Li C. Controlled synthesis of ultrathin hollow mesoporous carbon nanospheres for supercapacitor applications. Ind Eng Chem Res. 2014;53(8):3125-30. http://doi.org/10.1021/ie403950t.
12. Chen X, Kierzek K, Cendrowski K, Pelech I, Zhao X, Feng J, et al. CVD generated mesoporous hollow carbon spheres as supercapacitors. Colloids Surf A Physicochem Eng Asp. 2012;396:246-50. http://doi.org/10.1016/j.colsurfa.2012.01.002.
13. Liu C, Wang J, Li J, Luo R, Shen J, Sun X, et al. Controllable synthesis of functional hollow carbon nanostructures with dopamine as precursor for supercapacitors. ACS Appl Mater Interfaces. 2015;7(33):18609-17. http://doi.org/10.1021/acsami.5b05035. PMid:26243663.
14. Shrestha LK, Wei Z, Subramaniam G, Shrestha RG, Singh R, Sathish M, et al. Nanoporous hollow carbon spheres derived from fullerene assembly as electrode materials for high-performance supercapacitors. Nanomaterials (Basel). 2023;13(5):946. http://doi.org/10.3390/nano13050946. PMid:36903824.
15. Gutiérrez-García CJ, Ambriz-Torres JM, Contreras-Navarrete JJ, Granados-Martínez FG, García-Ruiz DL, García-González L, et al. Synthesis of carbon spheres by atmospheric pressure chemical vapor deposition from a serial of aromatic hydrocarbon precursors. Physica E Low Dimens Syst Nanostruct. 2019;112:78-85. http://doi.org/10.1016/j.physe.2019.04.007.
16. Stöber W, Fink A, Bohn E. Controlled growth of monodisperse silica spheres in the micron size range. J Colloid Interface Sci. 1968;26(1):62-9. http://doi.org/10.1016/0021-9797(68)90272-5.
17. Liu J, Qiao SZ, Liu H, Chen J, Orpe A, Zhao D, et al. Extension of the Stöber method to the preparation of monodisperse resorcinol-formaldehyde resin polymer and carbon spheres. Angew Chem Int Ed Engl. 2011;50(26):5947-51. http://doi.org/10.1002/anie.201102011. PMid:21630403.
18. Greasley SL, Page SJ, Sirovica S, Chen S, Martin RA, Riveiro A, et al. Controlling particle size in the Stöber process and incorporation of calcium. J Colloid Interface Sci. 2016;469:213-23. http://doi.org/10.1016/j.jcis.2016.01.065. PMid:26890387.
19. Elkhatat AM, Al-Muhtaseb SA. Advances in tailoring resorcinol-formaldehyde organic and carbon gels. Adv Mater. 2011;23(26):2887-903. http://doi.org/10.1002/adma.201100283. PMid:21608048.
20. Kakunuri M, Sharma CS. Resorcinol-formaldehyde derived carbon xerogels: A promising anode material for lithium-ion battery. J Mater Res. 2018;33(9):1074-87. http://doi.org/10.1557/jmr.2017.461.
21. Liu Y, Sun Y, Cho K, Ahn H-J, Ahn J-H. Entrapping polysulfides using mesoporous carbon hollow spheres with controlled internal SiO_2 content for lithium–sulfur batteries. J Mater Sci. 2023;58(17):7418-28. http://doi.org/10.1007/s10853-023-08430-6.
22. Fuertes AB, Valle-Vigón P, Sevilla M. One-step synthesis of silica@resorcinol–formaldehyde spheres and their application for the fabrication of polymer and carbon capsules. Chem Commun (Camb). 2012;48(49):6124-6. http://doi.org/10.1039/c2cc32552g. PMid:22582187.
23. de Oliveira RAG, Zanoni TB, Bessegato GG, Oliveira DP, Umbuzeiro GA, Zanoni MVB. A química e toxicidade dos corantes de cabelo. Quim Nova. 2014;37:1037-46. http://doi.org/10.5935/0100-4042.20140143.
24. Braghiroli FL, Amaral-Labat G, Boss AFN, Lacoste C, Pizzi A. Tannin gels and their carbon derivatives: a review. Biomolecules. 2019;9(10):587. http://doi.org/10.3390/biom9100587. PMid:31597350.
25. Quílez-Bermejo J, Pérez-Rodríguez S, Celzard A, Fierro V. Progress in the use of biosourced phenolic molecules for electrode manufacturing. Front Mater. 2022;9:810575. http://doi.org/10.3389/fmats.2022.810575.
26. Ogawa S, Yazaki Y. Tannins from Acacia mearnsii De Wild. Bark: Tannin Determination and Biological Activities. Molecules. 2018;23(4):837. http://doi.org/10.3390/molecules23040837. PMid:29621196.
27. Beda A, Rabuel F, Rahmouni O, Morcrette M, Matei Ghimbeu C. Optimization of tannin-derived hard carbon spheres for high-performance sodium-ion batteries. J Mater Chem A Mater Energy Sustain. 2023;11(8):4365-83. http://doi.org/10.1039/D2TA07951H.
28. Peres RS, Armelin E, Alemán C, Ferreira CA. Modified tannin extracted from black wattle tree as an environmentally friendly antifouling pigment. Ind Crops Prod. 2014;65:506-14. http://doi.org/10.1016/j.indcrop.2014.10.033.
29. Peres RS, Cassel E, Azambuja DS. Black Wattle Tannin as steel corrosion inhibitor. Int Sch Res Notices. 2012;1:937920. http://doi.org/10.5402/2012/937920.
30. Moraes NP, Goes CM, Rocha RS, Gouvêa MEV, de Siervo A, Silva MLCP, et al. Tannin-based carbon xerogel as a promising co-catalyst for photodegradation processes based on solar light: a case study using the tin (IV) oxide/carbon xerogel composite. Chem Eng Commun. 2022;209(11):1570-82. http://doi.org/10.1080/00986445.2021.1978076.
31. Moreira WM, Viotti PV, Vieira MGA, dos Santos CMGB, Scaliante MHNO, Gimenes ML. Hydrothermal synthesis of biobased carbonaceous composite from a blend of kraft black liquor and tannin and its application to aspirin and paracetamol removal.

Colloids Surf A Physicochem Eng Asp. 2021;608:125597. http://doi.org/10.1016/j.colsurfa.2020.125597.
32. Braghiroli FL, Fierro V, Izquierdo MT, Parmentier J, Pizzi A, Celzard A. Nitrogen-doped carbon materials produced from hydrothermally treated tannin. Carbon. 2012;50(15):5411-20. http://doi.org/10.1016/j.carbon.2012.07.027.
33. Mikova NM, Ivanov IP, Zhizhaev AM, Tsyganova SI, Kuznetsov BN. Synthesis and properties of carbon gels based on larch Bark Tannins and Hydrolysis Lignin. Russ J Appl Chem. 2022;95(3):393-400. http://doi.org/10.1134/S1070427222030089.
34. Koopmann AK, Torres-Rodríguez J, Salihovic M, Schoiber J, Musso M, Fritz-Popovski G, et al. Tannin-based nanoscale carbon spherogels as electrodes for electrochemical applications. ACS Appl Nano Mater. 2021;4(12):14115-25. http://doi.org/10.1021/acsanm.1c03431. PMid:34977479.
35. Liu M, Cai C, Li J, Zhao J, Teng W, Liu R. Stöber synthesis of tannic acid-formaldehyde resin polymer spheres and their derived carbon nanospheres and nanocomposites for oxygen reduction reaction. J Colloid Interface Sci. 2018;528:1-9. http://doi.org/10.1016/j.jcis.2018.05.070. PMid:29803955.
36. Yang I, Jung M, Kim MS, Choi D, Jung JC. Physical and chemical activation mechanisms of carbon materials based on the microdomain model. J Mater Chem A Mater Energy Sustain. 2021;9(15):9815-25. http://doi.org/10.1039/D1TA00765C.
37. Liu C, Wang J, Li J, Hu X, Lin P, Shen J, et al. Controllable synthesis of N-doped hollow-structured mesoporous carbon spheres by an amine-induced Stöber-silica/carbon assembly process. J Mater Chem A Mater Energy Sustain. 2016;4(30):11916-23. http://doi.org/10.1039/C6TA03748H.
38. Li S, Pasc A, Fierro V, Celzard A. Hollow carbon spheres, synthesis and applications – a review. J Mater Chem A Mater Energy Sustain. 2016;4(33):12686-713. http://doi.org/10.1039/C6TA03802F.
39. Zhang S, Wu J, Wang J, Qiao W, Long D, Ling L. Constructing *T*-Nb2O5@Carbon hollow core-shell nanostructures for high-rate hybrid supercapacitor. J Power Sources. 2018;396:88-94. http://doi.org/10.1016/j.jpowsour.2018.06.007.
40. Brunauer S, Emmett PH, Teller E. Adsorption of gases in multimolecular layers. J Am Chem Soc. 1938;60(2):309-19. http://doi.org/10.1021/ja01269a023.
41. Thommes M, Kaneko K, Neimark AV, Olivier JP, Rodriguez-Reinoso F, Rouquerol J, et al. Physisorption of gases, with special reference to the evaluation of surface area and pore size distribution (IUPAC Technical Report). Pure Appl Chem. 2015;87(9-10):1051-69. http://doi.org/10.1515/pac-2014-1117.
42. Dubinin MM. Fundamentals of the theory of adsorption in micropores of carbon adsorbents: characteristics of their adsorption properties and microporous structures. Carbon. 1989;27(3):457-67. http://doi.org/10.1016/0008-6223(89)90078-X.
43. Stoller MD, Ruoff RS. Best practice methods for determining an electrode material's performance for ultracapacitors. Energy Environ Sci. 2010;3(9):1294-301. http://doi.org/10.1039/c0ee00074d.
44. Li C, Wu W, Wang P, Zhou W, Wang J, Chen Y, et al. Fabricating an Aqueous Symmetric Supercapacitor with a Stable High Working Voltage of 2 V by Using an Alkaline–Acidic Electrolyte. Adv Sci (Weinh). 2018;6(1):1801665. http://doi.org/10.1002/advs.201801665. PMid:30643731.
45. Beda A, Rabuel F, Rahmouni O, Morcrette M, Matei Ghimbeu C. Optimization of tannin-derived hard carbon spheres for high-performance sodium-ion batteries. J Mater Chem A Mater Energy Sustain. 2023;11(8):4365-83. http://doi.org/10.1039/D2TA07951H.
46. Yao H, Zhang J, Du J, Li B, Zong S, Chen A. Carbon spheres prepared by amino acid-catalyzed resorcinol-formaldehyde polymerization for supercapacitors. J Alloys Compd. 2022;26:166948. http://doi.org/10.1016/j.jallcom.2022.166948.
47. Chun Y, Zhu Y, Stubenrauch C, Lu Y, Rojas OJ. Biobased ordered porous materials in the nano-to microscales. Curr Opin Colloid Interface Sci. 2024;73:101822. http://doi.org/10.1016/j.cocis.2024.101822.
48. Amaral-Labat G, Szczurek A, Fierro V, Celzard A. Unique bimodal carbon xerogels from soft templating of tannin. Mater Chem Phys. 2015;150:193-201. http://doi.org/10.1016/j.matchemphys.2014.10.006.
49. Castro-Gutiérrez J, Celzard A, Fierro V. Energy storage in supercapacitors: focus on tannin-derived carbon electrodes. Front Mater. 2020;7:217. http://doi.org/10.3389/fmats.2020.00217.
50. Tuinstra F, Koenig JL. Raman spectrum of graphite. J Chem Phys. 1970;53(3):1126-30. http://doi.org/10.1063/1.1674108.
51. De Falco G, Bocchicchio S, Commodo M, Minutolo P, D'Anna A. Raman spectroscopy of nascent soot oxidation: structural analysis during heating. Front Energy Res. 2022;10:878171. http://doi.org/10.3389/fenrg.2022.878171.
52. Guo T, Huo P, Li L, Wang Z, Guo L. Amorphous materials emerging as prospective electrodes for electrochemical energy storage and conversion. Chem. 2023;9(5):1080-93. http://doi.org/10.1016/j.chempr.2023.03.032.
53. Mai LQ, Minhas-Khan A, Tian X, Hercule KM, Zhao YL, Lin X, et al. Synergistic interaction between redox-active electrolyte and binder-free functionalized carbon for ultrahigh supercapacitor performance. Nat Commun. 2013;4(1):2923. http://doi.org/10.1038/ncomms3923. PMid:24327172.
54. Castro-Gutiérrez J, Sanchez-Sanchez A, Ghanbaja J, Díez N, Sevilla M, Celzard A, et al. Synthesis of perfectly ordered mesoporous carbons by water-assisted mechanochemical self-assembly of tannin. Green Chem. 2018;20(22):5123-32. http://doi.org/10.1039/C8GC02295J.
55. Castro-Gutiérrez J, Díez N, Sevilla M, Izquierdo MT, Celzard A, Fierro V. Model carbon materials derived from tannin to assess the importance of pore connectivity in supercapacitors. Renew Sustain Energy Rev. 2021;151:111600. http://doi.org/10.1016/j.rser.2021.111600.
56. Baig MM, Gul IH, Baig SM, Shahzad F. The complementary advanced characterization and electrochemical techniques for electrode materials for supercapacitors. J Energy Storage. 2021;44(Pt A):103370. http://doi.org/10.1016/j.est.2021.103370.
57. George J, Balachandran M. Extrinsic pseudocapacitance: tapering the borderline between pseudocapacitive and battery type electrode materials for energy storage applications. J Energy Storage. 2023;74(Pt A):109292. http://doi.org/10.1016/j.est.2023.109292.
58. Rodríguez-Rego JM, Macías-García A, Mendoza-Cerezo L, Díaz-Parralejo A, Carrasco-Amador JP. Design, machining and characterization of the components required for the manufacture of a supercapacitor. J Energy Storage. 2023;73(Pt C):109110. http://doi.org/10.1016/j.est.2023.109110.
59. Wang Y, Zhang L, Hou H, Xu W, Duan G, He S, et al. Recent progress in carbon-based materials for supercapacitor electrodes: a review. J Mater Sci. 2021;56:173-200. http://doi.org/10.1007/s10853-020-05157-6.
60. Díez N, Ferrero GA, Sevilla M, Fuertes AB. A sustainable approach to hierarchically porous carbons from tannic acid and their utilization in supercapacitive energy storage systems. J Mater Chem A Mater Energy Sustain. 2019;7(23):14280-90. http://doi.org/10.1039/C9TA01712G.
61. Guizani C, Widsten P, Siipola V, Paalijärvi R, Berg J, Pasanen A, et al. New insights into the chemical activation of lignins and tannins using K_2CO_3: a combined thermoanalytical and structural study. Carbon Lett. 2024;34(1):371-86. http://doi.org/10.1007/s42823-023-00601-4.
62. Malik A, Lenzen M, Li M, Mora C, Carter S, Giljum S, et al. Polarizing and equalizing trends in international trade and Sustainable Development Goals. Nat Sustain. 2024;7(10):1359-70. http://doi.org/10.1038/s41893-024-01397-5.

Data Availability

The dataset supporting the results of this study is not publicly available.